Title

Intermixing at the In x S y /Cu2ZnSn(S,Se)4 Heterojunction and Its Impact on the Chemical and Electronic Interface Structure

Journal

ACS Applied Energy Materials, 2(6)

ISSN

2574-0962

Authors

Hauschild, D
Mezher, M
Schnabel, T
et al.

Publication Date

2019-06-24

DOI

10.1021/acsaem.9b00263

Peer reviewed

Intermixing at the $In_xS_y/Cu_2ZnSn(S,Se)_4$ Heterojunction and its Impact on the Chemical and Electronic Interface Structure

D. Hauschild[1,2,3*], M. Mezher[3,#], T. Schnabel[4], S. Spiering[4], W. Kogler[4],
J. Carter[3], M. Blum[3,5], W. Yang[5], E. Ahlswede[4], C. Heske[1,2,3], and
L. Weinhardt[1,2,3,*]

[1] Institute for Photon Science and Synchrotron Radiation (IPS), Karlsruhe Institute of Technology (KIT), Hermann-v.-Helmholtz-Platz 1, 76344 Eggenstein-Leopoldshafen, Germany

[2] Institute for Chemical Technology and Polymer Chemistry (ITCP), Karlsruhe Institute of Technology (KIT), Engesserstr. 18/20, 76128 Karlsruhe, Germany

[3] Department of Chemistry and Biochemistry, University of Nevada, Las Vegas (UNLV), 4505 Maryland Parkway, Las Vegas, NV 89154-4003, USA

[4] Zentrum für Sonnenenergie- und Wasserstoff-Forschung Baden-Württemberg (ZSW), Meitnerstraße 1, 70563 Stuttgart, Germany

[5] Advanced Light Source (ALS), Lawrence Berkeley National Laboratory, 1 Cyclotron Road, Berkeley, CA 94720, USA

*Authors to whom correspondence should be addressed: dirk.hauschild@kit.edu, lothar.weinhardt@kit.edu

Current Affiliation: General Atomics, 3550 General Atomics Ct., San Diego, CA 92121

Keywords: Kesterite, Thin-Film Solar Cell, Indium Sulfide, Band Alignment, Photoelectron Spectroscopy, Inverse Photoemission Spectroscopy, X-ray Emission Spectroscopy, Electronic Structure

Abstract

We report on the chemical and electronic structure of the interface between a thermally co-evaporated In_xS_y buffer and a $Cu_2ZnSn(S,Se)_4$ (CZTSSe) absorber for thin-film solar cells that, to date, has achieved energy conversion efficiencies up to 8.6 %. Using surface-sensitive x-ray and UV photoelectron spectroscopy, combined with inverse photoemission and bulk-sensitive soft x-ray emission spectroscopy, we find a complex character of the buffer layer. It includes oxygen, as well as selenium and copper that diffused from the absorber into the In_xS_y buffer, exhibits an electronic band gap of 2.50 ± 0.18 eV at the surface, and leads to a small cliff in the conduction band alignment at the In_xS_y/CZTSSe interface. After an efficiency-increasing annealing step at 180 °C in nitrogen atmosphere, additional selenium diffusion leads to a reduced band gap at the buffer layer surface (2.28 ± 0.18 eV).

I Introduction

$Cu_2ZnSn(S,Se)_4$ (CZTSSe, “kesterite”), composed of earth-abundant elements, has attracted intensive research interest as an absorber material for thin-film solar cells [1–5]. For highest efficiencies, a CdS buffer layer is used, usually deposited via chemical bath deposition. However, the limited band gap of CdS (2.4 eV) leads to parasitic high-energy photon losses in the CdS buffer layer [6]. Hence, promising alternatives like indium sulfide [4,7] or zinc oxysulfide [Zn(O,S)] [8,9] with larger band gaps (and different interface chemistries) are being investigated. Such alternative buffer layers are intensively pursued for the (related) $Cu(In,Ga)(S,Se)_2$ material system, and there is a growing interest to also investigate the impact of alternative buffer layers on the kesterite-based solar cell [5,6,10–12]. In fact, the (to-date) significantly lower conversion efficiency of kesterite-based devices allows the speculation that other buffers might be better suited than the “standard” CdS developed for $Cu(In,Ga)(S,Se)_2$-based cells.

Apart from the differences of the buffer material properties, the interface between the buffer and the absorber film is expected to play an important role for the completed device, both with respect to the chemical (e.g., local bonding and intermixing) as well as electronic properties (e.g., the band alignment). In the case of the In_xS_y/CIGSSe interface, a diffusion of copper and selenium into the indium sulfide buffer has been reported previously [7,13,14]. Here, we present a detailed analysis of the chemical and electronic structure of the In_xS_y/CZTSSe interface. To investigate an additional, efficiency-increasing process step, the In_xS_y surface of a completed heterojunction after annealing in a nitrogen-filled glove box was also analyzed. For the analysis of the chemical structure, soft x-ray emission spectroscopy (XES) and x-ray photoelectron spectroscopy (XPS) were employed. To determine the valence and conduction band alignment at the buffer/absorber interface, we additionally used ultra-violet photoelectron spectroscopy (UPS) and inverse photoemission spectroscopy (IPES).

II Experimental

At the ZSW, CZTSSe absorbers were prepared from solution, using metal salts, thiourea, and dimethyl sulfoxide (DMSO) as solvent. The precursor solution was deposited onto a molybdenum substrate by doctor-blading and subsequently annealed under Se-atmosphere for 15 minutes at 550°C, resulting in chemical composition ratios of Cu/(Zn+Sn) = 0.85 and Zn/Sn = 1.24. For further details, the reader is referred to Ref. [1]. The absorbers were stored for several days in a nitrogen-filled glovebox, and indium sulfide (In_xS_y) buffer layers with different thicknesses (up to 25 nm) were then thermally evaporated from an In_2S_3 powder at a pressure of ~10^{-6} mbar. The thickness of the In_xS_y layers was estimated based on the evaporation time and reflectivity measurements.

Six identical cells with this layer structure were processed by adding 40 nm intrinsic ZnO (i-ZnO) and a 400 nm aluminum-doped ZnO (ZnO:Al) layer[15]. Devices with the corresponding glass/Mo/CZTSSe/In_xS_y/i-ZnO/ZnO:Al structure achieved efficiencies of up to η = 6.3 %. After a short (15 minutes, 180°C in air) annealing step of the full solar cell, the short circuit current density J_{SC} decreases from 36.1 mA/cm² by ~9 %, while the open circuit voltage V_{OC} increases from 426 to 436 mV and the fill factor (FF) from 40.6 to 60.0 %. This leads to an efficiency increase (up) to 8.6 %, which is the highest reported efficiency (to date) for a CZTSSe-based cell with indium sulfide buffer. The current density-voltage curves and parameters of the best device are shown in the Supporting Information (SI). To investigate the influence of this annealing step on the interface, it was mimicked by annealing a 25 nm In_xS_y/CZTSSe interface sample in a nitrogen-filled glovebox (for 15 min at 180 °C in N_2).

Samples for surface analysis were sealed under nitrogen atmosphere and shipped to UNLV for XPS, UPS, and IPES measurements. There, the samples were transferred into ultra-high vacuum (UHV) without additional air exposure. XPS (Mg and Al K_α) and UPS (He I and II) measurements were

performed with a SPECS PHOIBOS 150 MCD electron analyzer. The analyzer was calibrated according to Ref. [16] using sputter-cleaned Au, Ag, and Cu reference foils. The Au foil was also used to calibrate the Fermi energy for UPS and IPES measurements. For the XPS/UPS/IPES measurements, the $Cu_2ZnSn(S,Se)_4$ absorber sample was cleaned with a 50 eV Ar^+-ion treatment for a total of 60 minutes (two 30-minute treatments). The 25 nm In_xS_y/CZTSSe and the *N_2-annealed* 25 nm In_xS_y/CZTSSe samples were cleaned for 30 minutes, while the intermediate buffer layer/CZTSSe samples were studied as-received (i.e., without treatment). XPS measurements after each cleaning step confirm that the Ar^+-ion treatment removes C and O contaminations without the formation of metallic phases [17–20], which are commonly found when sputter-cleaning at higher ion energies. IPES spectra were recorded using a Staib low-energy electron gun and a custom-built Dose-type detector with I_2:Ar filling. After taking the XPS, UPS, and IPES dataset, the samples were again sealed under nitrogen atmosphere and shipped to the ALS. The XES measurements were performed at Beamline 8.0.1, using the SALSA endstation [21]. The S $L_{2,3}$ XES spectra were calibrated using a CdS single crystal reference [22].

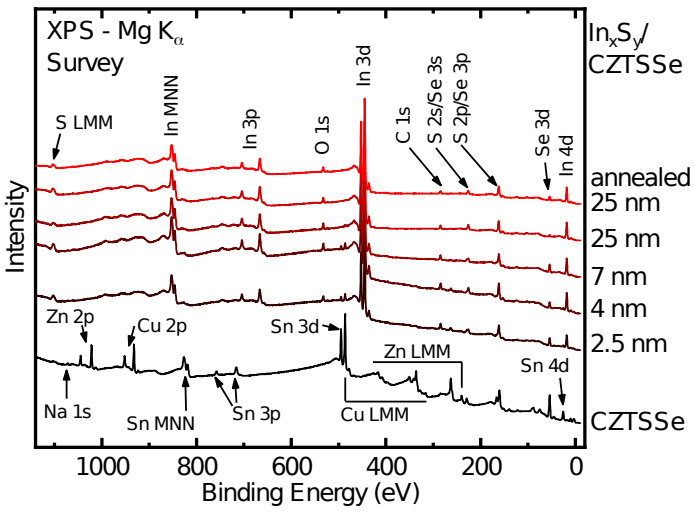

Fig. 1: XPS survey spectra of the CZTSSe absorber and the 2.5, 4, 7, and 25 nm In_xS_y/CZTSSe samples, as well as a 25 nm In_xS_y/CZTSSe sample after

annealing in N_2 at 180 °C. Prominent photoelectron and Auger features are labeled.

III Results and Discussion

Figure 1 shows the XPS survey spectra of the In_xS_y/CZTSSe sample series with increasing buffer layer thickness from bottom to top. The most prominent photoelectron and Auger lines are labeled. For the spectrum of CZTSSe, peaks related to all absorber elements (e.g., Cu 2p, Zn 2p, Sn 3d, S LMM, Se 3d), as well as a small Na 1s peak, are clearly visible. As for chalcopyrite-based thin-film solar cells [23,24], sodium diffuses from the soda-lime glass substrate into the back contact, the absorber, and to the absorber surface during the absorber preparation process. It is known to play a crucial role for the performance of kesterite-based solar cells [25,26]. Very low C 1s and O 1s signals suggest that the vast majority of carbon- and oxygen-related adsorbates was successfully removed during the ion treatment. For increasing In_xS_y thickness, the absorber-related peaks are increasingly attenuated - for the 7 nm In_xS_y/CZTSSe sample, most of the absorber peaks are no longer visible, which suggests a closed In_xS_y layer on the CZTSSe absorber. In parallel, In- and S-related peaks become more prominent. Furthermore, small selenium and sodium signals are still found on the 25 nm In_xS_y/CZTSSe surface. After the annealing step at 180 °C, the Se 3d signal increases by a factor of ~3, while the sodium intensity remains constant. This suggests selenium diffusion upon deposition and, additionally, after the annealing step. For $Cu(In,Ga)(S,Se)_2$ thin-film solar cells, selenium is found to diffuse into In_xS_y buffer layers[27]. The same behavior occurs for kesterites, which will be demonstrated in more detail below. In contrast to the absorber, a small O 1s and C 1s signal is detected for all buffer layer samples even after the ion treatment.

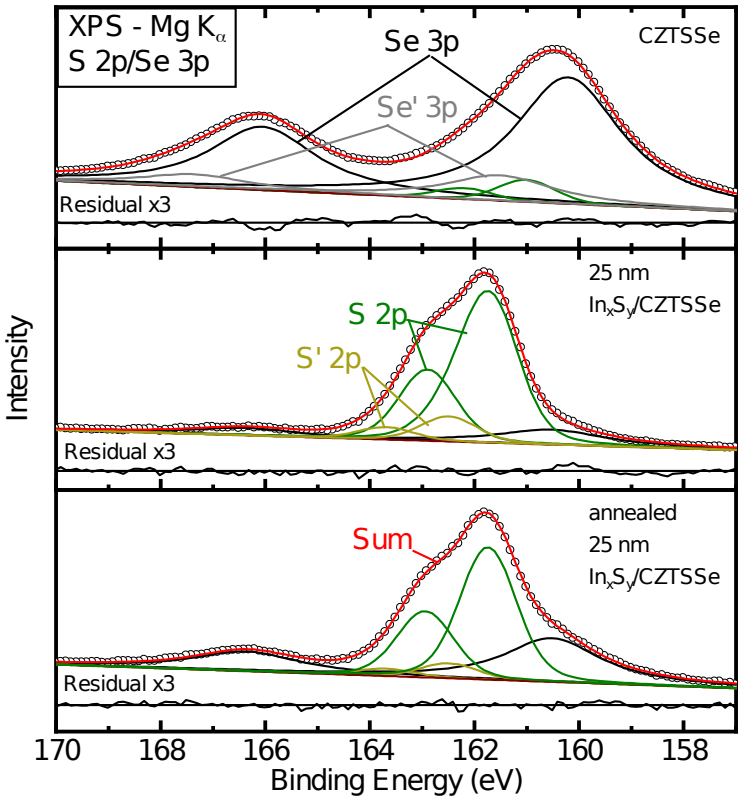

Fig 2. Top to bottom: S 2p/Se 3p XPS spectra of the CZTSSe absorber, the 25 nm In_xS_y/CZTSSe sample, and the annealed 25 nm In_xS_y/CZTSSe sample. The fit visualizes the different spectral components, and the magnified (x3) residual is shown below each spectrum.

To gain a more detailed picture of selenium diffusion into the In_xS_y buffer layer, we analyze the S 2p/Se 3p core level region. For this purpose, we have fitted the corresponding photoelectron features with a linear background function and several Voigt profiles. For the simultaneous fit of the dataset, the Gaussian and Lorentzian widths for each spin-orbit doublet were coupled, their intensity ratio was fixed to 2:1 (according to the multiplicity 2j+1), and the spin-orbit splitting was also used as a fit parameter (resulting in a S 2p and Se 3p spin-orbit splitting of 1.19 eV and 5.84 eV, respectively). The resulting fits for the absorber, the 25 nm In_xS_y/CZTSSe, and the annealed 25 nm In_xS_y/CZTSSe sample are shown in Figure 2. The CZTSSe absorber spectrum needs to be fitted with a S 2p doublet and two Se 3p doublets (the

second doublet is marked with a prime in Fig. 2). The first Se species (black, Se $3p_{3/2}$ at 160.2 eV) can likely be assigned to a selenide compound (e.g., CZTSSe) [28]. The second species (Se' $3p_{3/2}$ at 161.5 eV) can tentatively be assigned to selenium in an oxidized environment, while also an elemental Se environment has been reported for such binding energies [29,30]. Accordingly, a second Se component is also found in the Se *3d* line of the CZTSSe absorber (not shown; the second Se $3d_{5/2}$ line is shifted by 1.7 eV, from 54.0 to 55.7 eV). The sulfur $2p_{3/2}$ peak at 161.0 eV matches the energetic position of sulfur in a sulfide environment [17].

For increasing buffer layer thickness, the selenium peaks are attenuated and the sulfur peaks gain in intensity (as expected). For the 25 nm In_xS_y/CZTSSe sample, the main S $2p_{3/2}$ peak is shifted by 0.73 eV (relative to the CZTSSe absorber) to 161.7 eV, indicating a different sulfide environment in the buffer. This is supported by the modified indium Auger parameter α'_{In} of the 25 nm In_xS_y/CZTSSe sample of (852.5 ± 0.1) eV, which suggests the presence of Cu-In-S bonds [16,31,32]. For all In_xS_y samples, a second S 2p component at higher binding energies is detected, which nevertheless still matches the energy region of sulfides. We speculate that this S 2p component belongs to a second In_xS_y-like phase (e.g., In_6S_7 [7] or $CuIn_5S_8$ [13]) or to sulfide in the vicinity of oxygen (e.g., as a next-nearest neighbor).

As mentioned above, a small Se 3p signal is also detected for the 25 nm In_xS_y/CZTSSe sample. After the 180°C annealing step (i.e., for the annealed 25 nm In_xS_y/CZTSSe sample, bottom spectrum in Fig. 2), the Se 3p signal contribution becomes more pronounced, revealing an annealing-induced Se diffusion. In contrast, no Sn or Zn signals are detected at the In_xS_y surface, ruling out the creation of pinholes/cracks in the buffer film.

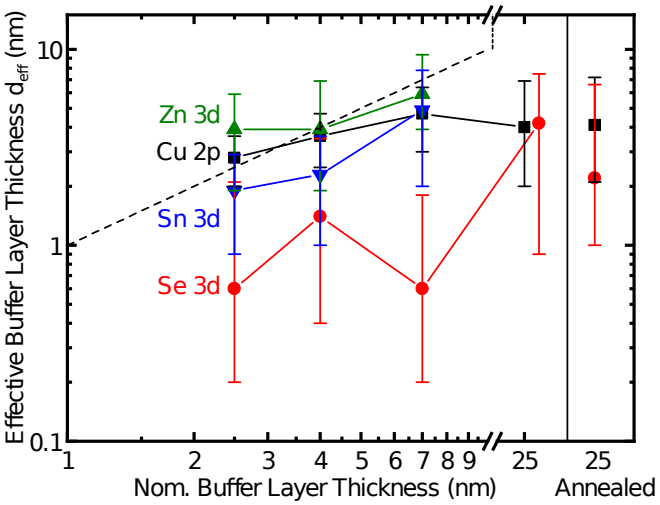

FIG 3: Effective buffer layer thickness d_{eff}, calculated from the attenuation of different absorber-related peaks, as a function of the nominal buffer layer thickness, estimated from the buffer layer growth time. The effective buffer layer thickness for the Se 3d peak lies significantly below the dashed line, indicating its diffusion during buffer layer growth as well as after annealing. For clarity, the 25 nm Se 3d data point is slightly shifted to the right.

In order to obtain a more detailed picture of the diffusion process, we calculate an "effective buffer layer thickness" from the attenuation of the most prominent absorber-related peaks. Assuming a buffer layer of homogeneous thickness d and no diffusion, the intensity of an XPS line is expressed by $I = I_0 \times e^{-d/\lambda}$, where I_0 is the line intensity for the absorber sample and λ the inelastic mean free path (IMFP), which was calculated using QUASES-IMFP [33,34]. Based on this, we define an "effective buffer layer thickness" as $d_{eff} = \lambda \ln(I_0/I)$ and plot it in Fig. 3 vs. the nominal buffer layer thickness as estimated from the buffer deposition time. If no diffusion occurs, the "effective buffer layer thickness" should be equal to the nominal buffer layer thickness, which is marked by the dashed line in Fig. 3. The values derived from the Zn and Sn 3d peaks agree with this line within the error bars, suggesting no diffusion of these elements. While the Cu 2p values also

lie on this line for buffer layer thicknesses up to (including) 7 nm, a small Cu 2p peak is still visible for the 25 nm In_xS_y/CZTSSe sample. The attenuation analysis derives an effective thickness of 4 nm, well below the nominal value of 25 nm, suggesting a weak copper diffusion into the In_xS_y buffer layer. It should be noted that we do not see any *additional* copper diffusion upon annealing (Fig. 3, right), which is indicated by the same "effective buffer layer thickness" as for the non-annealed sample. Earlier studies on *chalcopyrite*-based interfaces show a strong impact of annealing on the copper diffusion [7,13,14]. Those studies used annealing temperatures around 200 °C, while, for the present study, 180 °C was used.

The "effective buffer layer thickness" calculated from the *selenium* 3d peak attenuation lies significantly below the dashed line for all samples, which clearly indicates selenium diffusion during the buffer layer growth. After annealing, the calculated effective buffer layer thickness further decreases, which points towards an additional selenium diffusion upon annealing. Note that some earlier studies on In_xS_y buffer layers also found a selenium diffusion [13,27], while others did not [7,14,32,35]. Please note that, at room temperature, indium sulfide crystalizes in the β-In_2S_3 phase with a high number of vacancies. They can easily host other atoms[36], e.g., Na[27] or Cu[7] and possibly Se.

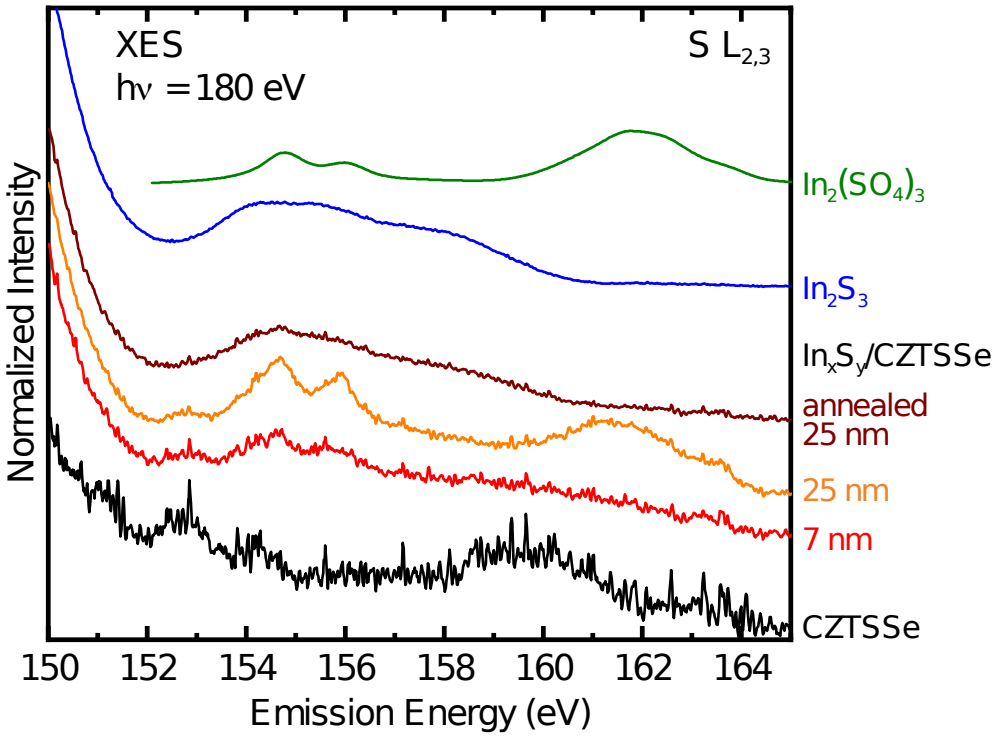

FIG 4: Non-resonant (hν = 180 eV) S $L_{2,3}$ XES spectra of the upper valence band region of the CZTSSe absorber, the 7 and 25 nm In_xS_y/CZTSSe samples, as well as the annealed 25 nm In_xS_y/CZTSSe sample. The spectra of $In_2(SO_4)_3$ and co-evaporated In_2S_3 reference samples are shown for comparison.

To study the chemical environment of the S atoms also with increased probing depth, we investigated the samples with XES. Here, the incoming and outgoing x-rays undergo an 1/e attenuation with attenuation lengths λ_{in} = 53 nm and λ_{out} = 260 nm, respectively[37]. The S $L_{2,3}$ XES signal of the upper valence band region (150 - 165 eV emission energy) of the CZTSSe absorber, and of the 7 nm, 25 nm, as well as the annealed 25 nm In_xS_y/CZTSSe samples, are shown in Figure 4. In addition, the spectra of an indium sulfate [$In_2(SO_4)_3$] reference powder and a co-evaporated indium sulfide (In_2S_3) film are shown. The low sulfur content in the CZTSSe absorber sample results in a lower signal-to-noise ratio for the bottommost spectrum. The CZTSSe absorber spectrum contains several characteristic emission features [2]. They can be assigned to electronic transitions from hybridized bands of the upper

valence region into the S 2p core holes. Accordingly, the region from 150 – 155 eV emission energy is dominated by Zn 3d-derived states and hybridized Sn 5s-S 3p states, indicating S-Zn and S-Sn bonds, respectively. The region from 158 – 162 eV is dominated by hybridized Cu 3d-S 3p states, thus indicative for S-Cu bonds. With increasing In_xS_y thickness, the spectral signature changes, now also containing contributions from S-In bonds (as discussed in conjunction with Fig. 5 below). Furthermore, three additional features can be seen; two sharp features at ~154.7 eV and ~156.0 eV, and a broad feature at ~ 161.5 eV with a shoulder at ~163.5 eV. These features are most prominent for the 25 nm In_xS_y/CZTSSe sample and can be attributed to sulfur atoms in an oxide environment (e.g., sulfate) [38–40]. We show $In_2(SO_4)_3$ as a reference for these S-O bonds (note that the formation of other sulfates and compounds with lower oxidation state might also contribute, especially for the shoulder at ~163.5 eV [41]). After the annealing step, the spectral signature of the S-O bonds is removed.

In order to quantify the S $L_{2,3}$ XES spectra, we have fitted them with a sum of the CZTSSe absorber and the In_2S_3 and the $In_2(SO_4)_3$ references. This is exemplarily shown for the 25 nm In_xS_y/CZTSSe and the annealed 25 nm In_xS_y/ CZTSSe films in Figure 5a) and b), respectively. The resulting weight factors of the three components are shown in Figure 5c). With increasing buffer layer thickness, the CZTSSe weight factor decreases (as expected) and those of In_2S_3 and $In_2(SO_4)_3$ increase. For the 25 nm In_xS_y/CZTSSe sample, the sulfate component is stronger than that of In_2S_3. After the annealing step, the sulfate fraction is significantly reduced, and the spectrum consists mainly of the In_2S_3 component (76%). We explain this as follows: Oxygen is built into the buffer layer (as oxides, hydroxides, and/or water), which is highlighted in the finding of S-O bonds. The annealing then likely reduces the oxygen content in the film, leading to a reduced contribution of S-O bonds to the spectrum of the (annealed) buffer layer.

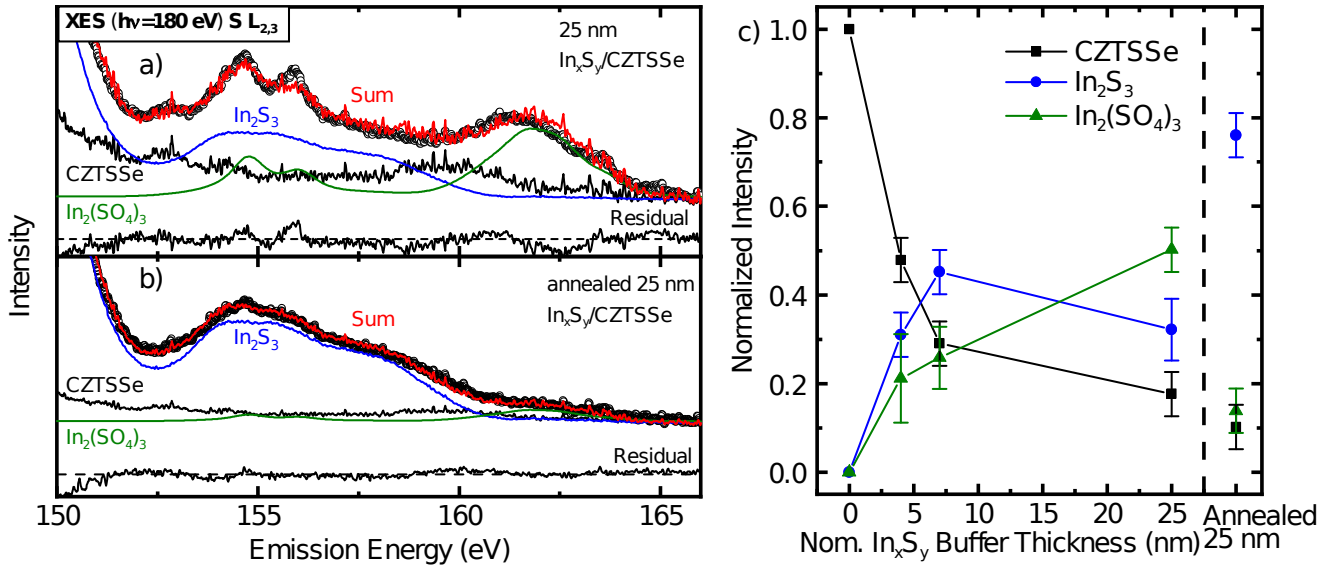

FIG 5: Three-component fit to reproduce a) the 25 nm In_xS_y/CZTSSe and b) the annealed 25 nm In_xS_y/CZTSSe S $L_{2,3}$ XES spectra. The residuals are shown below each panel. c) The resulting weight factors of the three-component fit as a function of buffer layer thickness.

In order to determine the band alignment at the In_xS_y/CZTSSe interface and to investigate the impact of the annealing on the electronic structure, we have used UPS and IPES and combined them with an XPS analysis of the core level positions. The UPS and IPES spectra of the ion-treated CZTSSe, 25 nm In_xS_y/CZTSSe, and annealed 25 nm In_xS_y/CZTSSe samples are shown on a common energy axis relative to E_F in Fig. 6. The valence band maximum (VBM) and conduction band minimum (CBM) were determined with a linear extrapolation of the leading edge of the respective spectrum [42,43].

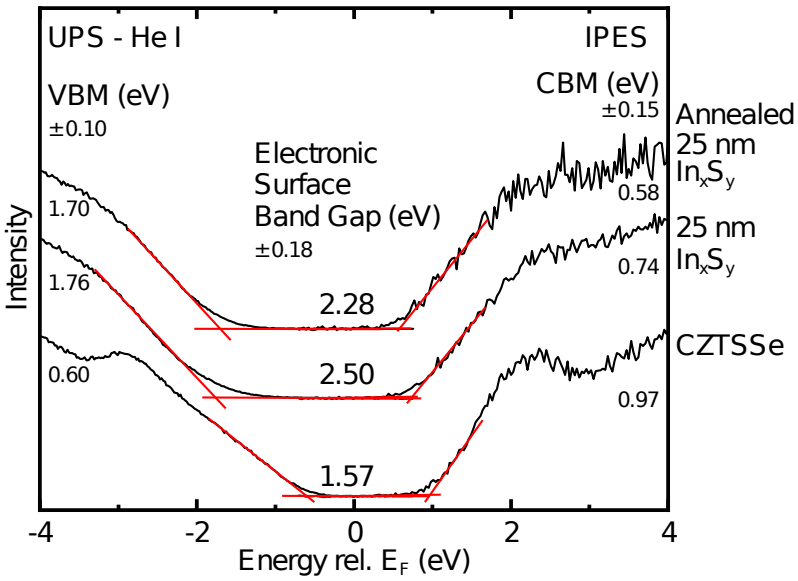

FIG 6: UPS and IPES spectra of the $Cu_2ZnSn(S,Se)_4$ absorber, the 25 nm In_xS_y/CZTSSe, and the annealed 25 nm In_xS_y/CZTSSe sample. All sample surfaces were cleaned with a 50 eV Ar^+ ion treatment. The spectra are plotted relative to the Fermi level, and all values are given in eV.

For the CZTSSe absorber, we derive the VBM and CBM to 0.60 ± 0.10 eV and 0.97 ± 0.15 eV, respectively. These positions indicate that the absorber's downward band bending towards the surface is relatively weak. The sum of VBM and CBM, i.e., the electronic band gap *at the surface* (1.57 ± 0.18 eV), is larger than the expected bulk band gap value of about ~1.1 eV [1]. Such an increased surface band gap was found before for chalcopyrites [18,44] and kesterites [45,46] and can be attributed to a stoichiometry variation (often: a copper depletion) at the surface.

In the UPS spectra of the non-annealed and annealed 25 nm In_xS_y/CZTSSe samples, a tail is detected at about 1.8 eV that is larger than the experimental resolution. This can possibly be related to defect states close to the VBM or to real In_xS_y states. A few published studies also show this broadening [32,47], while others do not [27,48]. For other wide-gap conductive materials [(Zn,Mg)O], we have recently [49] interpreted such tails as

electronically active states that contribute to the excellent charge carrier transport, while the dominant edges in the UPS and IPES spectra are assigned to the optically relevant edges, giving rise to the wide-band gap character and transparency.

In our case, we have refrained from such a detailed analysis for the buffer layer, as these tails, at most, might lead to an overestimation of the buffer surface band gap and possibly impact the determination of the valence band offset (VBO). In contrast, the determination of the conduction band offset (CBO), which is the main focus of this interface alignment analysis, is not affected.

For the non-annealed 25 nm In_xS_y/CZTSSe sample, we determine the VBM and CBM to 1.76 ± 0.10 eV and 0.74 ± 0.15 eV, respectively, leading to an electronic surface band gap of 2.50 ± 0.18 eV. This value is slightly larger than the commonly reported literature values of ~2.2 - 2.4 eV for In_2S_3 and can be related to the presence of oxygen in the film, which is found to increase the In_2S_3 band gap [50], and possibly to the above-discussed broadening at the VBM.

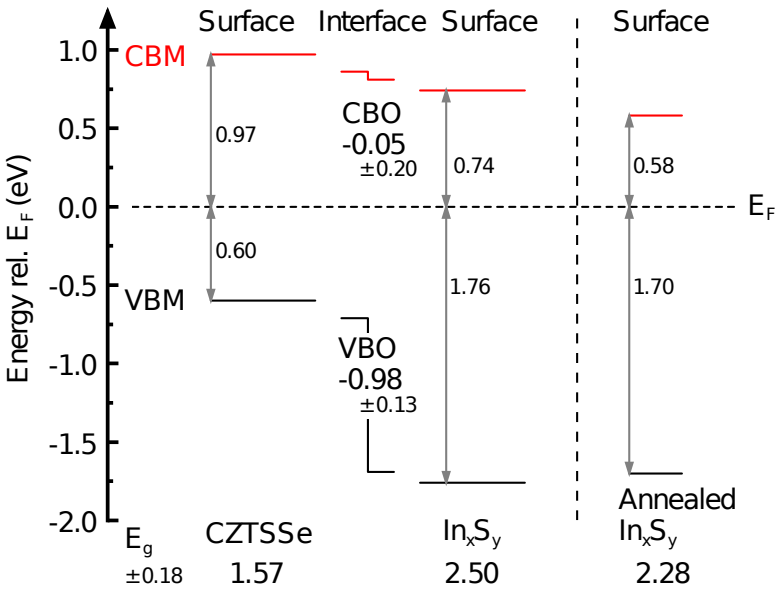

FIG 7: Derived band alignment for the In_xS_y/CZTSSe interface (left), and VBM/ CBM positions of the annealed In_xS_y/CZTSSe surface (right). A small cliff in the conduction band (-0.05 ± 0.20 eV) is found for the non-annealed interface. After annealing, the CBM of the buffer is shifted downwards, while the VBM is relatively unaffected. Electronic surface band gaps (E_g) are listed underneath each surface depiction. All values are given in eV.

To derive the band alignment, possible changes in the band edge positions induced by the formation of the interface need to be considered. For this purpose, we used the 2.5 and 4 nm buffer layers and measured the shifts of the absorber core levels as a function of buffer layer thickness. Here, we exclusively used the Sn 3d and Zn 3d lines, since copper- and selenium-related core levels might be influenced by the diffusion discussed above. The band bending in the buffer layer was evaluated by determining the relative shift of the In 3d and S 2p core levels for the thin buffer layer samples with respect to the 25 nm In_xS_y/CZTSSe sample. On average, we find a shift of -0.11 ± 0.08 eV and 0.07 ± 0.06 eV for the absorber- and buffer-related core levels, respectively. Based on this, we are able to derive the band alignment of the In_xS_y/CZTSSe interface, which is shown in Fig 7. We find a small cliff in the conduction band alignment (-0.05 ± 0.20) eV and a significant valence band offset (hole barrier) of (-0.98 ± 0.13) eV, respectively. Note that, within the error bars, a description with a “flat” conduction band alignment would also be applicable.

The impact of annealing on the VBM of the 25 nm In_xS_y/CZTSSe sample is small (+0.06 ± 0.05 eV), while a clear (-0.16 ± 0.05 eV) downward shift of the CBM (to 0.58 ± 0.15 eV) is found. Thus, we find a significantly smaller electronic surface band gap of 2.28 ± 0.18 eV for the annealed buffer. This decrease could be due to the reduction of oxygen in the film after the annealing step, as seen in the XES spectra in Figs. 4 and 5. Furthermore, the

diffusion of Se (energy gap of In_2Se_3 ~ 1.5 eV [51]) could decrease the band gap of the buffer layer.

Since the buffer layer thickness is significantly larger than λ, it is not possible to access the buried In_xS_y/CZTSSe interface, and hence it is not possible to determine the CBM and VBM of the annealed CZTSSe “surface”. The observed downward shift of the CBM, at first sight, would suggest an increase in the magnitude of the cliff (and hence an enhanced interface recombination). However, we point out that the observed Se diffusion, likely due to S/Se intermixing at the buffer/absorber interface[13,48,52,53], and the reduction of the amount of oxygen in the buffer layer might lead to a significantly altered interface alignment. This includes the fact that the offset might no longer be “vertical”, but smeared out along the compositional gradient at the junction.

It is reported[54–56] that a reduction of a cliff or even a change to a flat band alignment at the buffer/absorber interface can lead to an increase of the fill factor. We thus surmise that our findings lead to the significant increase of the fill factor and, hence, the increase in efficiency of the corresponding solar cells after the annealing process. Likely, the benefits of the annealing process also involve other aspects, beyond a simple view of the In_xS_y/CZTSSe interface band alignment.

IV Summary

In summary, we have investigated the chemical and electronic properties of the In_xS_y/CZTSSe interface before and after annealing. Upon deposition, we find a copper and selenium diffusion into the buffer layer. Furthermore, our XPS and XES analysis suggests a significant amount of oxygen in the In_xS_y buffer layer. This amount is strongly reduced by the annealing step. Without annealing, we find an electronic surface band gap of this buffer of 2.50 ± 0.18 eV and a small cliff alignment at the In_xS_y/CZTSSe interface. After the annealing step, the electronic surface band gap of the buffer layer is reduced

to 2.28 ± 0.18 eV, probably caused by a significant selenium diffusion and the reduction of the oxygen content in the layer.

Acknowledgements:

Funding by the German Federal Ministry of Education and Research (Free-InCa, 03SF0530B) is gratefully acknowledged. This research used resources of the Advanced Light Source, which is a DOE Office of Science User Facility under contract no. DE-AC02-05CH11231.

Supporting Information

J-V curves and parameters of the as-grown and annealed samples

References

(1) Schnabel, T.; Löw, M.; Ahlswede, E. Vacuum-Free Preparation of 7.5% Efficient $Cu_2ZnSn(S,Se)_4$ Solar Cells Based on Metal Salt Precursors. *Sol. Energy Mater. Sol. Cells* **2013**, *117*, 324–328 DOI: 10.1016/j.solmat.2013.06.021.

(2) Bär, M.; Schubert, B.-A.; Marsen, B.; Schorr, S.; Wilks, R. G.; Weinhardt, L.; Pookpanratana, S.; Blum, M.; Krause, S.; Zhang, Y.; Yang, W.; Unold, T.; Heske, C.; Schock, H.-W. Electronic Structure of Cu_2ZnSnS_4 Probed by Soft X-Ray Emission and Absorption Spectroscopy. *Phys. Rev. B* **2011**, *84*, 035308 DOI: 10.1103/PhysRevB.84.035308.

(3) Hages, C. J.; Levcenco, S.; Miskin, C. K.; Alsmeier, J. H.; Abou-Ras, D.; Wilks, R. G.; Bär, M.; Unold, T.; Agrawal, R. Improved Performance of Ge-Alloyed CZTGeSSe Thin-Film Solar Cells through Control of Elemental Losses: Improved Performance of CZTGeSSe Solar Cells. *Prog. Photovolt. Res. Appl.* **2015**, *23*, 376–384 DOI: 10.1002/pip.2442.

(4) Kim, J.; Hiroi, H.; Todorov, T. K.; Gunawan, O.; Kuwahara, M.; Gokmen, T.; Nair, D.; Hopstaken, M.; Shin, B.; Lee, Y. S.; Wang, W.; Sugimoto, H.; Mitzi, D. B. High Efficiency $Cu_2ZnSn(S,Se)4$ Solar Cells by Applying a Double In_2S_3/CdS Emitter. *Adv. Mater.* **2014**, *26*, 7427–7431 DOI: 10.1002/adma.201402373.

(5) Platzer-Björkman, C.; Frisk, C.; Larsen, J. K.; Ericson, T.; Li, S.-Y.; Scragg, J. J. S.; Keller, J.; Larsson, F.; Törndahl, T. Reduced Interface Recombination in Cu_2ZnSnS_4 Solar Cells with Atomic Layer Deposition $Zn_{1-x}Sn_xO_y$ Buffer Layers. *Appl. Phys. Lett.* **2015**, *107*, 243904 DOI: 10.1063/1.4937998.

(6) Schnabel, T.; Seboui, M.; Bauer, A.; Choubrac, L.; Arzel, L.; Harel, S.; Barreau, N.; Ahlswede, E. Evaluation of Different Buffer Materials for Solar Cells with Wide-Gap $Cu_2ZnGeS_xSe_{4-x}$ Absorbers. *RSC Adv.* **2017**, *7*, 40105–40110 DOI: 10.1039/C7RA06438A.

(7) Hauschild, D.; Meyer, F.; Benkert, A.; Kreikemeyer-Lorenzo, D.; Pohlner, S.; Palm, J.; Blum, M.; Yang, W.; Wilks, R. G.; Bär, M.; Heske, C.; Weinhardt, L.; Reinert, F. Annealing-Induced Effects on the Chemical Structure of the In_2S_3/$CuIn(S,Se)_2$ Thin-Film Solar Cell Interface. *J. Phys. Chem. C* **2015**, *119*, 10412–10416 DOI: 10.1021/acs.jpcc.5b01622.

(8) Platzer-Björkman, C.; Törndahl, T.; Abou-Ras, D.; Malmström, J.; Kessler, J.; Stolt, L. Zn(O,S) Buffer Layers by Atomic Layer Deposition in $Cu(In,Ga)Se_2$ Based Thin Film Solar Cells: Band Alignment and Sulfur Gradient. *J. Appl. Phys.* **2006**, *100*, 044506 DOI: 10.1063/1.2222067.

(9) Mezher, M.; Garris, R.; Mansfield, L. M.; Horsley, K.; Weinhardt, L.; Duncan, D. A.; Blum, M.; Rosenberg, S. G.; Bär, M.; Ramanathan, K.; Heske, C. Electronic Structure of the Zn(O,S)/$Cu(In,Ga)Se_2$ Thin-Film Solar Cell Interface. *Prog. Photovolt. Res. Appl.* **2016**, 1142–1148 DOI: 10.1002/pip.2764.

(10) Barkhouse, D. A. R.; Haight, R.; Sakai, N.; Hiroi, H.; Sugimoto, H.; Mitzi, D. B. Cd-Free Buffer Layer Materials on $Cu_2ZnSn(S_xSe_{1-x})_4$: Band Alignments with ZnO, ZnS, and In_2S_3. *Appl. Phys. Lett.* **2012**, *100*, 193904 DOI:

10.1063/1.4714737.
(11) Buffiere, M.; Barreau, N.; Brammertz, G.; Sahayaraj, S.; Meuris, M.; Poortmans, J. Development of Co-Evaporated In_2S_3 Buffer Layer for $Cu_2ZnSnSe_4$ Thin Film Solar Cells. In *Photovoltaic Specialist Conference (PVSC), 2015 IEEE 42nd*; 2015; pp 1–4.
(12) Hironiwa, D.; Matsuo, N.; Chantana, J.; Sakai, N.; Kato, T.; Sugimoto, H.; Minemoto, T. Annealing Effect on $Cu_2ZnSn(S,Se)_4$ Solar Cell with $Zn_{1-x}Mg_xO$ Buffer Layer. *Phys. Status Solidi A* **2015**, 1–6 DOI: 10.1002/pssa.201532217.
(13) Bär, M.; Barreau, N.; Couzinié-Devy, F.; Pookpanratana, S.; Klaer, J.; Blum, M.; Zhang, Y.; Yang, W.; Denlinger, J. D.; Schock, H.-W.; Weinhardt, L.; Kessler, J.; Heske, C. Nondestructive Depth-Resolved Spectroscopic Investigation of the Heavily Intermixed In_2S_3/Cu(In,Ga)Se_2 Interface. *Appl. Phys. Lett.* **2010**, *96*, 184101-184101–184103 DOI: doi:10.1063/1.3425739.
(14) Pistor, P.; Allsop, N.; Braun, W.; Caballero, R.; Camus, C.; Fischer, Ch.-H.; Gorgoi, M.; Grimm, A.; Johnson, B.; Kropp, T.; Lauermann, I.; Lehmann, S.; Mönig, H.; Schorr, S.; Weber, A.; Klenk, R. Cu in In_2S_3: Interdiffusion Phenomena Analysed by High Kinetic Energy X-ray Photoelectron Spectroscopy. *Phys. Status Solidi A* **2009**, *206*, 1059–1062 DOI: 10.1002/pssa.200881162.
(15) Powalla, M.; Dimmler, B. Process Development of High Performance CIGS Modules for Mass Production. *Thin Solid Films* **2001**, *387*, 251–256 DOI: 10.1016/S0040-6090(00)01708-9.
(16) Moulder, J. F.; Stickle, W. F.; Sobol, P. E.; Bomben, K. D. *Handbook of X-Ray Photoelectron Spectroscopy, Perkin-Elmer Corporation. Page 15*; Physical Electronics Division, 1992.
(17) Bär, M.; Schubert, B.-A.; Marsen, B.; Krause, S.; Pookpanratana, S.; Unold, T.; Weinhardt, L.; Heske, C.; Schock, H.-W. Native Oxidation and Cu-Poor Surface Structure of Thin Film Cu_2ZnSnS_4 Solar Cell Absorbers. *Appl. Phys. Lett.* **2011**, *99*, 112103 DOI: 10.1063/1.3637574.
(18) Morkel, M.; Weinhardt, L.; Lohmüller, B.; Heske, C.; Umbach, E.; Riedl, W.; Zweigart, S.; Karg, F. Flat Conduction-Band Alignment at the CdS/$CuInSe_2$ Thin-Film Solar-Cell Heterojunction. *Appl. Phys. Lett.* **2001**, *79*, 4482–4484 DOI: 10.1063/1.1428408.
(19) Weinhardt, L.; Heske, C.; Umbach, E.; Niesen, T. P.; Visbeck, S.; Karg, F. Band Alignment at the i-ZnO/CdS Interface in Cu(In,Ga)$(S,Se)_2$ Thin-Film Solar Cells. *Appl. Phys. Lett.* **2004**, *84*, 3175–3177 DOI: 10.1063/1.1704877.
(20) Weinhardt, L.; Fuchs, O.; Groß, D.; Storch, G.; Umbach, E.; Dhere, N. G.; Kadam, A. A.; Kulkarni, S. S.; Heske, C. Band Alignment at the CdS/Cu(In,Ga)S_2 Interface in Thin-Film Solar Cells. *Appl. Phys. Lett.* **2005**, *86*, 062109-062109–3 DOI: 10.1063/1.1861958.
(21) Blum, M.; Weinhardt, L.; Fuchs, O.; Bär, M.; Zhang, Y.; Weigand, M.; Krause, S.; Pookpanratana, S.; Hofmann, T.; Yang, W.; Denlinger, J. D.; Umbach, E.; Heske, C. Solid and Liquid Spectroscopic Analysis (SALSA)–a Soft x-Ray Spectroscopy Endstation with a Novel Flow-through Liquid Cell. *Rev. Sci. Instrum.* **2009**, *80*, 123102 DOI: 10.1063/1.3257926.
(22) Weinhardt, L.; Fuchs, O.; Fleszar, A.; Bär, M.; Blum, M.; Weigand, M.; Denlinger, J. D.; Yang, W.; Hanke, W.; Umbach, E.; Heske, C. Resonant

Inelastic Soft X-Ray Scattering of CdS: A Two-Dimensional Electronic Structure Map Approach. *Phys. Rev. B* **2009**, *79*, 165305 DOI: 10.1103/PhysRevB.79.165305.
(23) Braunger, D.; Hariskos, D.; Bilger, G.; Rau, U.; Schock, H. W. Influence of Sodium on the Growth of Polycrystalline Cu(In,Ga)Se_2 Thin Films. *Thin Solid Films* **2000**, *361–362*, 161–166 DOI: 16/S0040-6090(99)00777-4.
(24) Heske, C.; Fink, R.; Umbach, E.; Riedl, W.; Karg, F. Na-induced Effects on the Electronic Structure and Composition of Cu(In,Ga)Se_2 Thin-film Surfaces. *Appl. Phys. Lett.* **1996**, *68*, 3431–3433 DOI: 10.1063/1.115783.
(25) Abzieher, T.; Schnabel, T.; Hetterich, M.; Powalla, M.; Ahlswede, E. Source and Effects of Sodium in Solution-Processed Kesterite Solar Cells. *Phys. Status Solidi A* **2015**, 1–11 DOI: 10.1002/pssa.201532619.
(26) Hsieh, Y.-T.; Han, Q.; Jiang, C.; Song, T.-B.; Chen, H.; Meng, L.; Zhou, H.; Yang, Y. Efficiency Enhancement of $Cu_2ZnSn(S,Se)_4$ Solar Cells via Alkali Metals Doping. *Adv. Energy Mater.* **2016**, *6*, 1502386 DOI: 10.1002/aenm.201502386.
(27) Hauschild, D.; Meyer, F.; Benkert, A.; Kreikemeyer-Lorenzo, D.; Dalibor, T.; Palm, J.; Blum, M.; Yang, W.; Wilks, R. G.; Bär, M.; Reinert, F.; Heske, C.; Weinhardt, L. Improving Performance by Na Doping of a Buffer Layer—Chemical and Electronic Structure of the In_xS_y:Na/CuIn(S,Se)$_2$ Thin-Film Solar Cell Interface. *Prog. Photovolt. Res. Appl.* **2018**, *26*, 359–366 DOI: 10.1002/pip.2993.
(28) Bär, M.; Repins, I.; Weinhardt, L.; Alsmeier, J.-H.; Pookpanratana, S.; Blum, M.; Yang, W.; Heske, C.; Wilks, R. G.; Noufi, R. Zn–Se–Cd–S Interlayer Formation at the CdS/$Cu_2ZnSnSe_4$ Thin-Film Solar Cell Interface. *ACS Energy Lett.* **2017**, 1632–1640 DOI: 10.1021/acsenergylett.7b00140.
(29) Chen, G.; Yuan, C.; Liu, J.; Deng, Y.; Jiang, G.; Liu, W.; Zhu, C. Low Cost Preparation of Cu_2ZnSnS_4 and $Cu_2ZnSn(S_xSe_{1-x})_4$ from Binary Sulfide Nanoparticles for Solar Cell Application. *J. Power Sources* **2014**, *262*, 201–206 DOI: 10.1016/j.jpowsour.2014.03.075.
(30) Larsen, J. K.; Ren, Y.; Ross, N.; Särhammar, E.; Li, S.-Y.; Platzer-Björkman, C. Surface Modification through Air Annealing $Cu_2ZnSn(S,Se)_4$ Absorbers. *Thin Solid Films* **2017**, *633*, 118–121 DOI: 10.1016/j.tsf.2016.08.030.
(31) Cahen, D.; Ireland, P. J.; Kazmerski, L. L.; Thiel, F. A. X-ray Photoelectron and Auger Electron Spectroscopic Analysis of Surface Treatments and Electrochemical Decomposition of $CuInSe_2$ Photoelectrodes. *J. Appl. Phys.* **1985**, *57*, 4761–4771 DOI: 10.1063/1.335341.
(32) Sterner, J.; Malmström, J.; Stolt, L. Study on ALD In_2S_3/Cu(In,Ga)Se_2 Interface Formation. *Prog. Photovolt. Res. Appl.* **2005**, *13*, 179–193 DOI: 10.1002/pip.595.
(33) Seah, M. P.; Dench, W. A. Quantitative Electron Spectroscopy of Surfaces: A Standard Data Base for Electron Inelastic Mean Free Paths in Solids. *Surf. Interface Anal.* **1979**, *1*, 2–11 DOI: 10.1002/sia.740010103.
(34) Tougaard, S. QUASES (QUantitative Analysis of Surfaces by Electron Spectroscopy) http://www.quases.com/home/ (accessed May 02, 2019).
(35) Abou-Ras, D.; Kostorz, G.; Strohm, A.; Schock, H.-W.; Tiwari, A. N.

Interfacial Layer Formations between Cu(In,Ga)Se_2 and InxSy Layers. *J. Appl. Phys.* **2005**, *98*, 123512-123512–123517 DOI: 10.1063/1.2149166.
(36) Pistor, P.; Merino Álvarez, J. M.; León, M.; di Michiel, M.; Schorr, S.; Klenk, R.; Lehmann, S. Structure Reinvestigation of α-, β- and γ-In2S3. *Acta Crystallogr. Sect. B Struct. Sci. Cryst. Eng. Mater.* **2016**, *72*, 410–415 DOI: 10.1107/S2052520616007058.
(37) Gullikson, E. M. CXRO X-Ray Interactions With Matter http://henke.lbl.gov/optical_constants/ (accessed May 02, 2019).
(38) Reichardt, J.; Bär, M.; Grimm, A.; Kötschau, I.; Lauermann, I.; Sokoll, S.; Lux-Steiner, M. C.; Fischer, Ch.-H.; Heske, C.; Weinhardt, L.; Fuchs, O.; Jung, C.; Gudat, W.; Niesen, T. P.; Karg, F. Inducing and Monitoring Photoelectrochemical Reactions at Surfaces and Buried Interfaces in Cu(In,Ga)$(S,Se)_2$ Thin-Film Solar Cells. *Appl. Phys. Lett.* **2005**, *86*, 172102-172102–172103 DOI: 10.1063/1.1906309.
(39) Heske, C.; Groh, U.; Fuchs, O.; Umbach, E.; Franco, N.; Bostedt, C.; Terminello, L. J.; Perera, R. C. C.; Hallmeier, K. H.; Preobrajenski, A.; Szargan, R.; Zweigart, S.; Riedl, W.; Karg, F. X-Ray Emission Spectroscopy of Cu(In,Ga)$(S,Se)_2$-Based Thin Film Solar Cells: Electronic Structure, Surface Oxidation, and Buried Interfaces. *Phys. Status Solidi A* **2001**, *187*, 13–24 DOI: 10.1002/1521-396X(200109)187:1<13::AID-PSSA13>3.0.CO;2-D.
(40) Meisel, A., Leonhardt, G., Szargan R. *Röntgenspektren und chemische Bindung.*; Leipzig Geest & Portig 1977., 1977.
(41) Duncan, D. A.; Kephart, J. M.; Horsley, K.; Blum, M.; Mezher, M.; Weinhardt, L.; Häming, M.; Wilks, R. G.; Hofmann, T.; Yang, W.; Bär, M.; Sampath, W. S.; Heske, C. Characterization of Sulfur Bonding in CdS:O Buffer Layers for CdTe-Based Thin-Film Solar Cells. *ACS Appl. Mater. Interfaces* **2015**, *7*, 16382–16386 DOI: 10.1021/acsami.5b03503.
(42) Gleim, T.; Heske, C.; Umbach, E.; Schumacher, C.; Gundel, S.; Faschinger, W.; Fleszar, A.; Ammon, C.; Probst, M.; Steinrück, H.-P. Formation of the ZnSe/(Te/)GaAs(1 0 0) Heterojunction. *Surf. Sci.* **2003**, *531*, 77–85 DOI: 10.1016/S0039-6028(03)00439-4.
(43) Gleim, T.; Heske, C.; Umbach, E.; Schumacher, C.; Faschinger, W.; Ammon, C.; Probst, M.; Steinrück, H.-P. Reduction of the ZnSe/GaAs(100) Valence Band Offset by a Te Interlayer. *Appl. Phys. Lett.* **2001**, *78*, 1867–1869 DOI: 10.1063/1.1358366.
(44) Hauschild, D.; Handick, E.; Göhl-Gusenleitner, S.; Meyer, F.; Schwab, H.; Benkert, A.; Pohlner, S.; Palm, J.; Tougaard, S.; Heske, C.; Weinhardt, L.; Reinert, F. Band-Gap Widening at the Cu(In,Ga)$(S,Se)_2$ Surface: A Novel Determination Approach Using Reflection Electron Energy Loss Spectroscopy. *ACS Appl. Mater. Interfaces* **2016**, *8*, 21101–21105 DOI: 10.1021/acsami.6b06358.
(45) Bär, M.; Schubert, B.-A.; Marsen, B.; Krause, S.; Pookpanratana, S.; Unold, T.; Weinhardt, L.; Heske, C.; Schock, H.-W. Impact of KCN Etching on the Chemical and Electronic Surface Structure of Cu_2ZnSnS_4 Thin-Film Solar Cell Absorbers. *Appl. Phys. Lett.* **2011**, *99*, 152111 DOI: 10.1063/1.3650717.
(46) Bär, M.; Schubert, B.-A.; Marsen, B.; Wilks, R. G.; Pookpanratana, S.; Blum, M.; Krause, S.; Unold, T.; Yang, W.; Weinhardt, L.; Heske, C.; Schock,

H.-W. Cliff-like Conduction Band Offset and KCN-Induced Recombination Barrier Enhancement at the CdS/Cu_2ZnSnS_4 Thin-Film Solar Cell Heterojunction. *Appl. Phys. Lett.* **2011**, *99*, 222105 DOI: 10.1063/1.3663327.
(47) Schulmeyer, T.; Klein, A.; Kniese, R.; Powalla, M. Band Offset at the $CuGaSe_2$/In_2S_3 Heterointerface. *Appl. Phys. Lett.* **2004**, *85*, 961–963 DOI: 10.1063/1.1779340.
(48) Bär, M.; Barreau, N.; Couzinié-Devy, F.; Weinhardt, L.; Wilks, R. G.; Kessler, J.; Heske, C. Impact of Annealing-Induced Intermixing on the Electronic Level Alignment at the In_2S_3/Cu(In,Ga)Se_2 Thin-Film Solar Cell Interface. *ACS Appl. Mater. Interfaces* **2016**, *8*, 2120–2124 DOI: 10.1021/acsami.5b10614.
(49) Duncan, D. A.; Mendelsberg, R.; Mezher, M.; Horsley, K.; Rosenberg, S. G.; Blum, M.; Xiong, G.; Weinhardt, L.; Gloeckler, M.; Heske, C. A New Look at the Electronic Structure of Transparent Conductive Oxides—A Case Study of the Interface between Zinc Magnesium Oxide and Cadmium Telluride. *Adv. Mater. Interfaces* **2016**, *3*, 1600418 DOI: 10.1002/admi.201600418.
(50) Barreau, N. Indium Sulfide and Relatives in the World of Photovoltaics. *Sol. Energy* **2009**, *83*, 363–371 DOI: 10.1016/j.solener.2008.08.008.
(51) Julien, C.; Eddrief, M.; Kambas, K.; Balkanski, M. Electrical and Optical Properties of In2Se3 Thin Films. *Thin Solid Films* **1986**, *137*, 27–37 DOI: 10.1016/0040-6090(86)90191-4.
(52) Weinhardt, L.; Bär, M.; Pookpanratana, S.; Morkel, M.; Niesen, T. P.; Karg, F.; Ramanathan, K.; Contreras, M. A.; Noufi, R.; Umbach, E.; Heske, C. Sulfur Gradient-Driven Se Diffusion at the CdS/CuIn(S,$Se)_2$ Solar Cell Interface. *Appl. Phys. Lett.* **2010**, *96*, 182102-182102–182103 DOI: 10.1063/1.3425666.
(53) Pookpanratana, S.; Repins, I.; Bär, M.; Weinhardt, L.; Zhang, Y.; Félix, R.; Blum, M.; Yang, W.; Heske, C. CdS/Cu(In,Ga)Se_2 Interface Formation in High-Efficiency Thin Film Solar Cells. *Appl. Phys. Lett.* **2010**, *97*, 074101 DOI: 10.1063/1.3481405.
(54) Minemoto, T.; Matsui, T.; Takakura, H.; Hamakawa, Y.; Negami, T.; Hashimoto, Y.; Uenoyama, T.; Kitagawa, M. Theoretical Analysis of the Effect of Conduction Band Offset of Window/CIS Layers on Performance of CIS Solar Cells Using Device Simulation. *Sol. Energy Mater. Sol. Cells* **2001**, *67*, 83–88 DOI: 10.1016/S0927-0248(00)00266-X.
(55) Liu, X.; Sites, J. R. Calculated Effect of Conduction-band Offset on $CuInSe_2$ Solar-cell Performance. In *AIP Conference Proceedings*; AIP Publishing, 1996; Vol. 353, pp 444–452.
(56) Erfurth, F.; Grimm, A.; Palm, J.; Niesen, T. P.; Reinert, F.; Weinhardt, L.; Umbach, E. Direct Determination of the Band Alignment at the (Zn,Mg)O/CISSe Interface. *Appl. Phys. Lett.* **2011**, *98*, 142107 DOI: 10.1063/1.3565972.